Structure

Monitoring the conformational ensemble and lipid environment of a mechanosensitive channel under cyclodextrin-induced membrane tension

Graphical abstract

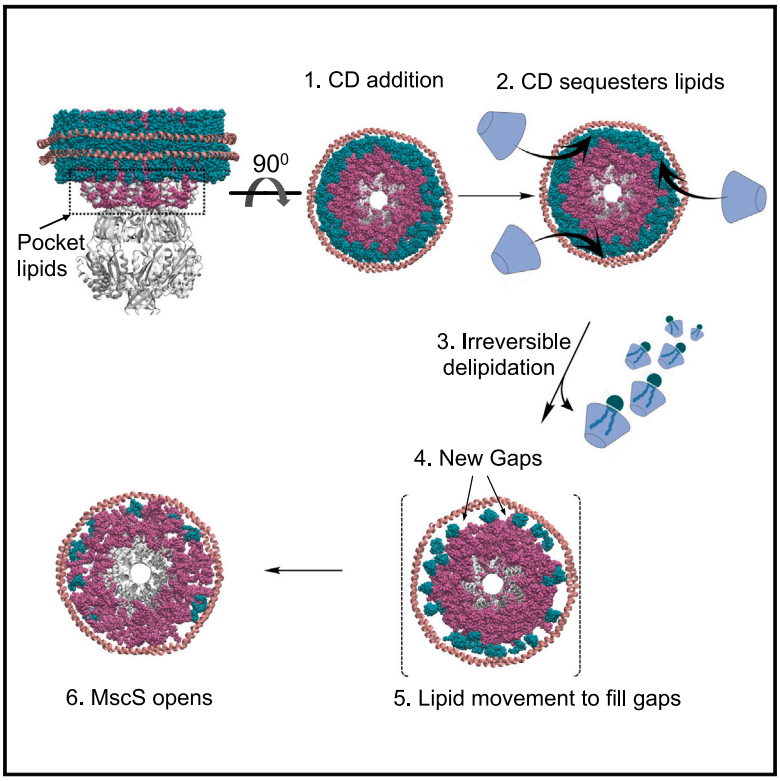

Authors

Benjamin J. Lane, Yue Ma, Nana Yan, ..., Theodoros K. Karamanos, Bela E. Bode, Christos Pliotas

Correspondence

christos.pliotas@manchester.ac.uk

In brief

Lane, Ma, Yan et al. demonstrate that the conformational ensemble of the mechanosensitive channel MscS can be monitored by EPR spectroscopy, the associated lipid environment by NMR, and single-channel transitions can be followed by electrophysiology under cyclodextrin-induced membrane tension.

Highlights

- Our approach allows the monitoring of tension-sensitive states in membrane proteins
- MscS conformational ensemble was probed by EPR spectroscopy under molecular tension
- The lipid environment within nanodiscs was monitored using NMR spectroscopy
- Electrophysiology measurements with cyclodextrin revealed MscS functional states

Lane et al., 2024, Structure *32*, 739–750
June 6, 2024
https://doi.org/10.1016/j.str.2024.02.020

CellPress

Structure

CellPress
OPEN ACCESS

Article

Monitoring the conformational ensemble and lipid environment of a mechanosensitive channel under cyclodextrin-induced membrane tension

Benjamin J. Lane,[1,6] Yue Ma,[2,6] Nana Yan,[1,6] Bolin Wang,[2] Katrin Ackermann,[3] Theodoros K. Karamanos,[4] Bela E. Bode,[3] and Christos Pliotas[1,2,5,7,*]

[1]Astbury Centre for Structural Molecular Biology, School of Biomedical Sciences, University of Leeds, Leeds LS2 9JT, UK
[2]School of Biological Sciences, Faculty of Biology, Medicine and Health, Manchester Academic and Health Science Centre, The University of Manchester, Manchester M13 9PT, UK
[3]EaStCHEM School of Chemistry, Biomedical Sciences Research Complex and Centre of Magnetic Resonance, University of St Andrews, St Andrews KY16 9ST, UK
[4]Department of Life Sciences, Faculty of Natural Sciences, Imperial College London, London SW7 2AZ, UK
[5]Manchester Institute of Biotechnology, The University of Manchester, Manchester M1 7DN, UK
[6]These authors contributed equally
[7]Lead contact
*Correspondence: christos.pliotas@manchester.ac.uk
https://doi.org/10.1016/j.str.2024.02.020

SUMMARY

Membrane forces shift the equilibria of mechanosensitive channels enabling them to convert mechanical cues into electrical signals. Molecular tools to stabilize and methods to capture their highly dynamic states are lacking. Cyclodextrins can mimic tension through the sequestering of lipids from membranes. Here we probe the conformational ensemble of MscS by EPR spectroscopy, the lipid environment with NMR, and function with electrophysiology under cyclodextrin-induced tension. We show the extent of MscS activation depends on the cyclodextrin-to-lipid ratio, and that lipids are depleted slower when MscS is present. This has implications in MscS' activation kinetics when distinct membrane scaffolds such as nanodiscs or liposomes are used. We find MscS transits from closed to sub-conducting state(s) before it desensitizes, due to the lack of lipid availability in its vicinity required for closure. Our approach allows for monitoring tension-sensitive states in membrane proteins and screening molecules capable of inducing molecular tension in bilayers.

INTRODUCTION

During their life cycle, cells must maintain osmotic balance while facing a myriad of environmental challenges in order to survive. During rainfall, bacteria accumulate water and experience extreme osmotic challenges. Bacterial mechanosensitive (MS) channels open in response to membrane tension and prevent cell lysis by acting as pressure safety valves.[1–5] If these pores remain open for prolonged periods of time, this leads to cell toxicity. MS channel activation is dependent on membrane physical properties such as tension, which relies on lipid movement to facilitate force transduction,[6–8] while molecular triggers are scarce, so the trapping of functional states remains a challenge. Monitoring their transitions would require ensemble methods that report on the state equilibria of large protein populations and single-molecule methods to access individual channel responses. The MS channel of small conductance MscS has served as a pivotal model system in understanding the function of bacterial and eukaryotic MS channels.[5,9–12] *Escherichia coli* MscS can adopt at least six conducting and three non-conducting states, but only four have been structurally characterized.[13–19] These intermediate state(s) are not only a unique feature of MscS but also play a role in the regulation of structurally diverse MS channels, such as the large-conductance MscL channel[20–24] as well as other MscS-like channels.[25–33] The MscS open state was first reported by Naismith, Booth et al.[18] and later confirmed in the native-like environment by electron paramagnetic resonance (EPR) spectroscopy.[34,35] Shortly after, a high-resolution structure identified lipids in cytoplasm-facing pockets, which act as negative allosteric modulators of MscS, leading to the proposal of the "lipid-moves-first" model.[6,9] This entropy-driven model[10] provided a molecular platform for the general force-from-lipid principle.[7] Lipids within similar pockets have been observed in a plethora of MS channels having key roles in their mechanical regulation.[9,14,16,17,20,21,26,28,32,33,36–38]

Initially used to remove cholesterol from cell membranes, β-cyclodextrin (CD) was able to stabilize MscS' functional states by mimicking membrane tension.[15,39,40] CD is able to deplete lipids, which induces movement of the remaining lipids, and this leads to tension generation within membranes. CD-to-lipid ratios spanning several orders of magnitude were used to activate MscS reconstituted in nanodiscs (NDs)[14] and giant

unilamellar vesicles (GUVs),[15] resulting in different time scales required for activation, between different techniques and lipid scaffolds used. To probe such phenomena, ensemble methods, such as pulse dipolar EPR and NMR spectroscopies, in which all protein and lipid molecules present in a given sample could be probed, are favored. Pulsed electron-electron double resonance (PELDOR, also known as DEER for double electron-electron resonance) spectroscopy has emerged as a powerful tool in the study of structural dynamics of membrane protein complexes.[21,35,41–50] This pulse dipolar EPR spectroscopy technique is usually combined with nitroxide-based spin labels engineered onto proteins to enable inter-spin distance measurements and deduce information on their conformational and oligomeric state(s).[51] NMR spectroscopy on the other hand is a sensitive and versatile tool, which can be used to monitor lipid changes, as well as membrane protein dynamics in real time.[52–55] Here, we combine PELDOR distance measurements to monitor shifts in the MscS conformational ensemble, with NMR spectroscopy to follow lipid movement under CD-induced molecular tension. We further employ single-channel electrophysiology to investigate the extent of MscS activation and alter the CD-to-lipid ratio to access intermediate sub-conducting states, essential to the tension-mediated pathway of MscS. We confirm by PELDOR that the MscS conformational ensemble shifts upon lipid depletion and further quantifies the associated lipid movement in real time by NMR. We further use similar conditions between our ensemble PELDOR/NMR and single-channel electrophysiology measurements in order to link channel structure with functional channel responses. We report that lipid depletion rates are dependent on MscS' presence, and these vary substantially between lipid ND and GUV scaffolds used for membrane protein reconstitution. Our integrative approach of ensemble magnetic resonance and single-molecule electrophysiology methods can be used to detect tension-sensitive states in membrane proteins and screen molecules generating membrane tension.

RESULTS

MscS activation extent depends on the CD-to-lipid ratio

Under naturally occurring tension, MscS could possess at least nine distinct states, namely three non-conducting: closed (C), desensitized (DS), and inactivated (IC), and six conducting (in an increasing based on their ion conductance order): sub-conducting one (S1), two (S2), three (S3), four (S4), five (S5), and a fully open (FO) state. While S1-S5 and FO states present different single-channel conductances, reflected by different conformations, it is debated whether the IC and DS non-conducting states adopt distinctive structural architectures.[16] To investigate the effect of molecular tension on individual MscS channels, we performed single-channel patch-clamp electrophysiology under increasing CD-to-lipid ratios. We implemented these measurements on the MscS D67R1 variant (D67C modified with MTSSL, (1-Oxyl-2,2,5,5-tetramethyl-3-pyrroline-3-methyl) methanethiosulfonate), since PELDOR requires the engineering of spin labels on MscS to obtain an EPR signal. Previously, patch-clamp electrophysiology recordings on MscS D67C performed in *E. coli* spheroplasts showed this variant is functional and with tension sensitivity and gating kinetics similar to wild-type (WT) MscS.[35] We first tested whether spin label modification has any effect on MscS function. To this end, we expressed, spin labeled, and reconstituted MscS D67R1 into Soy-PC GUVs and performed single-channel recordings under controlled membrane tension (n = 14) (Figure S1, where "n" is the number of independent patches tested hereafter). MscS channels opened with a mean unitary channel conductance of 0.78 ± 0.15 nS (n = 8) recorded at negative and 1.0 ± 0.1 nS (n = 6) at positive voltages. These activities were recorded at pressures ranging between −40 and −60 mmHg and are in agreement with WT MscS conductance, threshold, and dwell times we recorded in GUVs (n = 7, Table S1; Figure S1), as well as with previous reports on WT MscS.[56,57] Our control experiments on WT MscS performed under identical conditions to MscS D67R1 along with previous recordings on the WT channel conclude that neither the spin label modification nor the mutation on this site affects MscS function. After ensuring that our excised patches contain active MscS channels, we incubated them with CD and performed recordings at four CD-to-lipid ratios, 20:1, 600:1, 6,000:1, and 30,000:1. The range of ratios was selected to be consistent with previous high CD-to-lipid ratios reported for single-channel recordings in GUVs[15] and low ratios combined with shorter incubation times used to capture MscS structures in NDs by cryoelectron microscopy (cryo-EM).[14] Initially, all individual patches showed large multiple MscS channel activities following pressure application (n = 6) (Figure 1A). However, after incubation with CD (20:1 CD-to-lipid ratio), in three patches, we observed no activities while for the rest we recorded conductances ranging between (0.15 and 0.56) nS, with first openings observed after 10–15 min of CD addition. These activities are consistent with low S3-S5 MscS sub-conducting states (Figure 1E). After ∼3 h of CD incubation (Figure 1A), in half of our patches, and out of the initial fourteen open channels recorded, only three opened after tension reapplication, while channels in the rest of the patches showed no activity. In combination, electrophysiology data for this ratio suggest that the vast majority of channels become desensitized after opening to low-level sub-conducting states (S3-S5). At 600:1 CD-to-lipid ratio, we observed channel openings within 4–5 min of CD incubation, with a conductance of 0.2 ± 0.04 nS, at +30 mV (Figures 1B and 1E), and of 0.19 ± 0.06 nS, at −30 mV (Figure S2) (n = 6). Our findings are consistent with CD being able to generate molecular tension and activate MscS. However, as in our lowest (20:1) ratio, also for 600:1, we did not observe any full or high conductance openings; instead, we saw low sub-conducting state(s) which mostly resemble the S5 state[15] (Figures 1 and S2). The latter appears at pressure thresholds similar to those seen for the other MscS states, though with lower open probability, and it is yet to be structurally resolved. After ∼30 min incubation, tension beyond the MscS' pressure threshold was reapplied. For all our active channel containing patches, we observed no or minor MscS activity, suggesting the channel(s) entered a desensitized (or inactivated) state[14,16,17] (Figures 1 and S2). In some cases, we recorded no channel activities following incubation with CD, and when we reapplied pressure to the patches, no activities were elicited, suggesting MscS transitioned from the closed to the desensitized state, without entering any of its conducting states (n = 7) (Figure S2). At an order of magnitude higher CD-to-lipid ratio (6,000:1), we observed multiple single-channel openings after 2–5 min of CD addition, consistent with a large

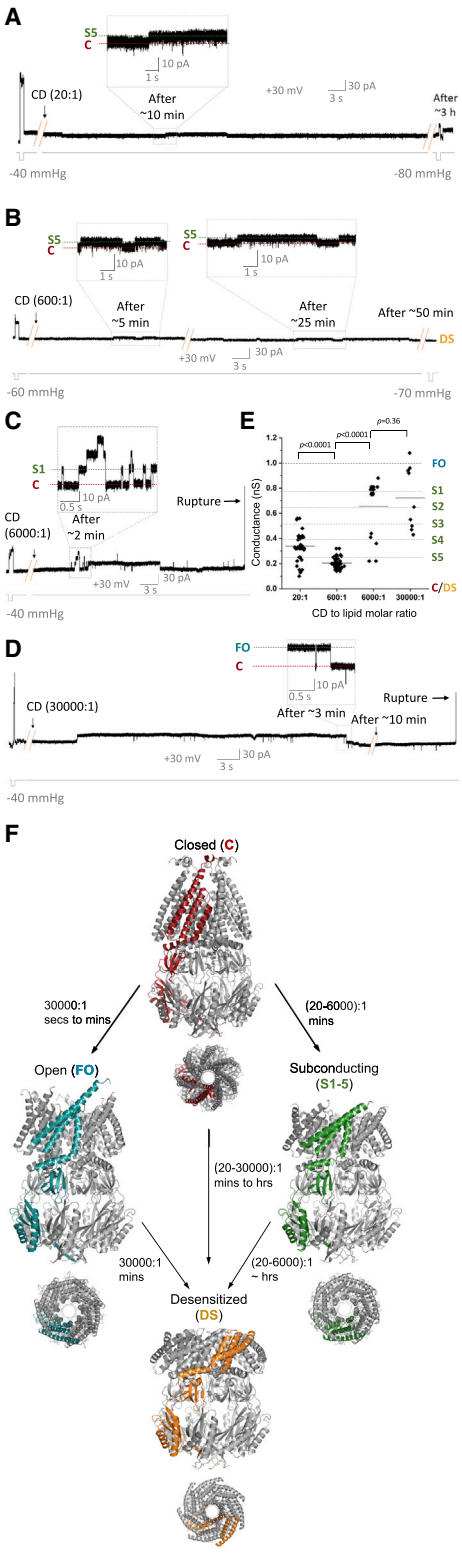

Figure 1. Tuning of CD-to-lipid ratio leads to distinct MscS-conducting states

Representative patch-clamp recordings of MscS D67R1 reconstituted into Soy-PC GUVs after perfusion with CD, recorded at +30 mV membrane potential.

range of MscS activities between 0.22–0.88 nS at +30 mV (Figures 1C and 1E) and 0.15–0.71 nS at −30 mV (Figure S2) (n = 8), in agreement with S1-S5 states. This time patches were fragile and ruptured after few minutes of CD incubation. An order of magnitude increase in the CD-to-lipid ratio has therefore heavily impacted MscS' range of activities and conducting states. Finally, we used the highest CD-to-lipid ratio (30,000:1), imposed by CD's inherent limited solubility. Although at this ratio the GUVs presented a high tendency for rupturing, we were successful in obtaining stable excised patches containing active MscS. This time we recorded a narrower range (compared to 6,000:1), but observed higher MscS conductances ranging between (0.43–1.08) nS at +30 mV (Figures 1D and 1E) and 0.48–0.81 nS at −30 mV (Figure S2) (n = 6), consistent with the high S1-S3 and FO MscS states. These openings appeared only within a couple of minutes of CD incubation and at an earlier time than in patches where lower ratios were used. Now patches ruptured after 10–15 min of CD incubation, not allowing for ∼ hours of single-channel recordings. Given that under these conditions and the CD-to-lipid ratio used, full opening(s) of MscS could be achieved, the molecular tension generated within the GUVs should be at least 7 mN/m required for MscS to reach full conductance.[8] For the lower CD-to-lipid ratios used for which we did not observe full openings, rather sub-openings of MscS, generated molecular tension should range between lipid-glass adhesion tension (0.5–4 mN/m)[58] and MscS pressure threshold, namely ∼4–7 mN/m. Taken together, our electrophysiology data indicate the extent of MscS activation depends on the CD-to-lipid ratio and MscS desensitizes after prolonged incubation with CD. Both MscS' transition pathways and gating kinetics depend on the CD-to-lipid ratio used, leading to MscS experiencing different lipid depletion rates (Figure 1F). We summarized the transitions MscS undergoes and the relative activation times for the different CD-to-lipid ratios in Figure 1F.

Probing the conformational ensemble of MscS by PELDOR spectroscopy

To probe the structural ensemble of MscS under molecular tension, we reconstituted channels into NDs and employed

(A) CD (20:1 CD-to-lipid molar ratio). Multiple channels were initially activated by −40 mmHg, then no channel activities were observed within 3 h of CD incubation, and finally, pressure was reapplied eliciting suppressed activities (after activation by CD, MscS desensitizes, i.e., becomes insensitive to applied negative pressure).

(B) CD (600:1 CD-to-lipid molar ratio). Channels were activated by −60 mmHg, followed by perfusion with CD, and then identical pressure protocols were applied with no MscS activity being elicited.

(C) CD (6,000:1 CD-to-lipid molar ratio). Channels were activated by −40 mmHg, followed by perfusion with CD, with multiple-channel openings observed prior to patch rupture.

(D) CD (30,000:1 CD-to-lipid molar ratio). Channels were activated by −40 mmHg with large single-channel openings observed prior to patch rupture.

(E) Distributions of resulting conductances of sub-states induced by CD with different CD-to-lipid molar ratios. Data represent unitary activities, and horizontal lines their mean values. Dash lines represent full openings (FO) and sub-states (S1-S5). The p values with unpaired t test comparison are indicated. n = 3 for each condition.

(F) Transitions observed in our electrophysiology setup under molecular tension using available MscS structures (side and top views). Closed, sub-conducting, desensitized (PDB: 6VYK/6VYL/6VYM),[14] and open (PDB: 5AJI).[9]

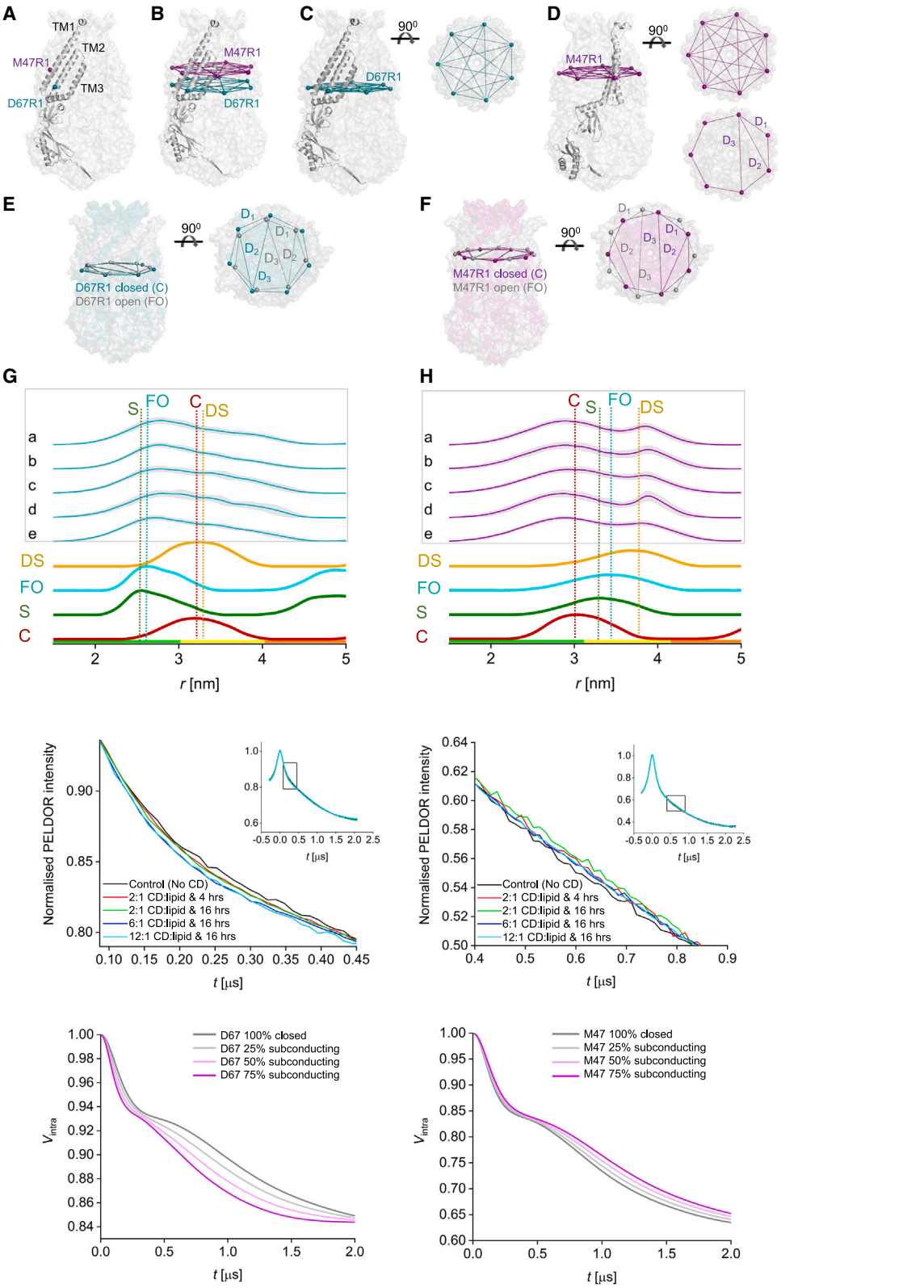

(legend on next page)

PELDOR in the presence of CD. We engineered two distinct spin reporters and measured distances to inform on changes in the equilibrium of MscS conformational states. Both MscS D67C and M47C form functional channels.[35] These sites are located in the transmembrane domain helices TM2 and TM1, respectively, and are able to discriminate between open/sub-conducting and closed/desensitized states (Figures 2A–2D). In MscS D67R1, distances shorten, while in contrast, MscS M47R1 distances increase when MscS transits from the closed toward the open state, due to an anti-clockwise rotation around channel z axis[18] (Figures 2E and 2F). We specifically selected these two reporting sites in order to account for any systematic errors.[34,35] For D67R1, a MscS structure with all seven spin labels resolved has been reported,[9] allowing for an accurate comparison with the PELDOR distances and complementing *in silico* distance modeling.

We expressed, spin labeled and reconstituted MscS D67R1 and M47R1 in 1,2-dioleoyl-*sn*-glycero-3-phosphocholine (DOPC) NDs. We selected membrane scaffold proteins (MSP)-formed NDs,[59] as they are well-established scaffolds for reconstituting membrane proteins to study in a lipid environment. DOPC was our lipid of choice to allow for direct comparison of our PELDOR data with modeled distances on MscS cryo-EM structures obtained in DOPC NDs.[14] Phosphatidylcholine (PC) lipids, also used in our electrophysiology experiments, are not native to *E. coli* but they are closely related to phosphatidylethanolamine (PE), the major component of *E. coli* membranes. Previously, MscS reconstituted in PC-containing NDs presented no functional differences to native *E. coli* lipid NDs,[16,17,34,37] or PE-containing GUVs[8,60] and our system could act as a model to investigate MscS' transitions under molecular tension.

Two CD molecules are required to remove one cholesterol or lipid molecule,[39,40] setting our minimum ratio tested here. For our PELDOR distance measurements, we incubated each of D67R1 and M47R1 for 4 and 16 h intervals at increasing CD-to-lipid ratios (2:1, 6:1, and 12:1), similar to the ones previously used to obtain cryo-EM structures.[14] We applied molecular tension by CD-induced lipid depletion and measured distances among the seven spins engineered onto our channels (one per monomer, assuming quantitative labeling) to obtain information on their conformation. Multi-spin effects in the PELDOR data were suppressed by reducing the inversion probability of the PELDOR pump pulse as described before.[61,62] In the absence of membrane tension, the obtained distance distributions show probabilities that cover all MscS states considered, although the distributions are consistent with a dominant contribution from the closed state, consistent with previous PELDOR and cryo-EM reports.[14,17,34,37] Following incubation of MscS with different CD ratios, the reaction was stopped, samples were collected, and then passed through size-exclusion chromatography to remove the excess of CD, empty NDs, and aggregates induced by CD interactions, prior to snap-freezing in liquid N_2. The predicted distance difference between the open and sub-conducting MscS is negligible for D67R1 and only a couple of Ångstroms for M47R1, thus we could not discriminate robustly between these two states from the distance distributions as differences are within the experimental uncertainties (Figures 2G and 2H) despite an excellent signal-to-noise ratio. However, the primary PELDOR data show an increased echo decay with increasing CD-to-lipid ratio for D67R1 and a decreased decay for M47R1. This is characteristic of a change in average distance. As the average distance increases, the dipolar coupling frequency reduces leading to a slower decay and vice versa. Our experimental data report a change in opposite directions for D67R1 and M47R1, with the average D67R1 distance reduced and the average M47R1 distance increased upon opening, in perfect agreement with predictions and previous studies.[34,35] This is also reproduced by exploratory simulations (Figures 2 and S3). It is important to note that *in silico* modeling is rarely exactly matching experiments but trends are often reproduced very well.[63] Thus, we refrain from fitting the distance distributions to a combination of states, given that also the number of states conceivable makes this likely underdetermined. Predicted distance differences between the closed and desensitized states are negligible for D67R1 but increase for M47R1, thus we conclude that no significant desensitization occurs under our PELDOR conditions as this would lead to larger changes in M47R1 and these are not observed (Figure S3). Note that the shift in distance distributions for conformational changes of a small fraction of channels within the entire ensemble was expected and we indeed found it to be very small (Figures 2G and 2H). If only small fractions of channels open, this will not be identifiable, due to uncertainty in the distance distributions, and all experimental distance distributions show distance probabilities reflecting all states considered (i.e., states for which high-resolution structures to model on are available).

Figure 2. Monitoring the conformational ensemble of MscS under molecular tension by PELDOR

(A) D67R1 (cyan spheres, TM2) and M47R1 (purple spheres, TM1) spin labeled reporters on MscS.

(B) Seven spin labels per single mutant site, owing to MscS' heptameric form. D67R1 (C) and M47R1 (D) side and top view in which all respective distances are shown (cyan and purple lines). (D) D_1, D_2, and D_3 distances due to MscS' heptameric symmetry are shown for clarity. Open (gray surface, PDB: 5AJI)[9] and (E) closed (cyan surface, PDB: 6VYK)[14] MscS showing the expected distance changes (gray and cyan lines) for D67R1 and (F) closed (purple surface, PDB: 6VYK) MscS showing the expected distance changes (gray and purple) for M47R1, including all possible distances for the two states. D67R1 distances reduce and M47R1 distances increase as MscS transits from the closed (cyan or purple surface) to the open state (gray surface), accounting for any systematic errors. MscS (G) D67R1 and (H) M47R1 PELDOR distance distributions under different CD conditions. D67R1 and M47R1 top five PELDOR data distributions and bottom four distributions showing the modeled distances for the closed ("C", dark red), sub-conducting ("S", green), fully open ("FO", cyan), and desensitized ("DS", gold) states with respective colored dash lines indicating the most probable distances based on our *in silico* modeling. CD-to-lipid ratios and incubation times used are: a) 12:1, 16 h, b) 6:1, 16 h, c) 2:1, 16 h, d) 2:1, 4 h, and e) initial state (control, no CD). Experimental traces (zoom) and modeled traces scaled with experimental modulation depth from control for different percentages of MscS sub-conducting state (PDB: 6VYL) populations within the ensemble for D67R1 (G column) and M47 (H column). PELDOR raw traces show similar trends to the simulated distributions. CD-to-lipid ratios for each sample are given in the respective figure legends. For PELDOR, the mean distance distributions (colored line) and ± 2σ confidence estimates (respective shaded colored areas) are shown calculated using the validation tool in DeerAnalysis. Traffic light indicates the reliability of PELDOR distribution: (green, shape reliable; yellow, mean and width reliable; orange, mean reliable). Y axis for distance distributions indicates the probability density P(r).

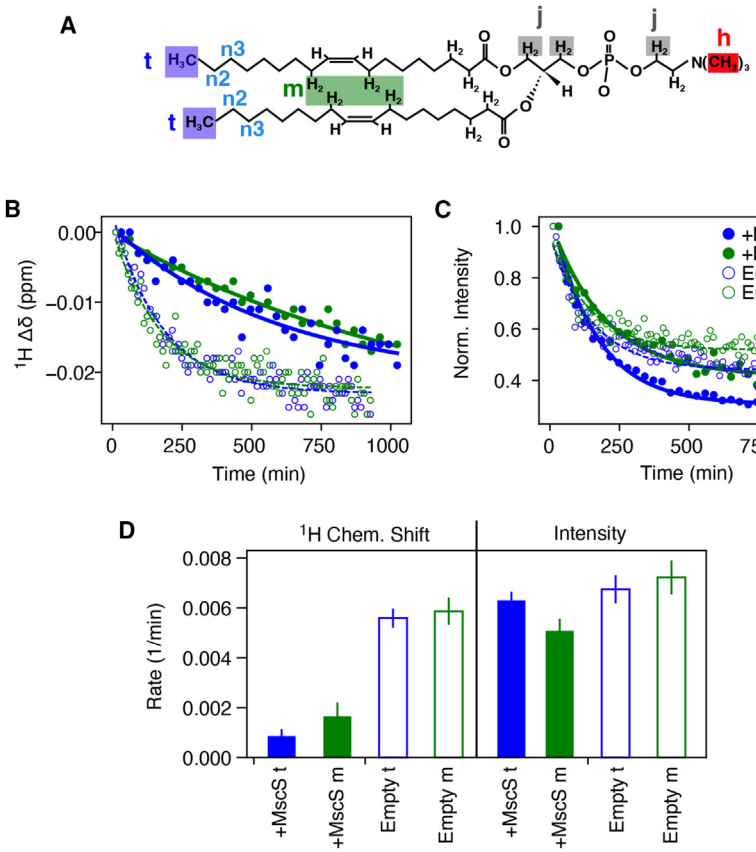

Figure 3. Probing the lipid environment of MscS in nanodiscs in the presence of cyclodextrin by NMR

A schematic of a DOPC lipid with highlighted boxes showing assigned resonances (A). The highlighted boxes on the DOPC lipid follow the same color coding as that of Figure S4A. Plots of proton chemical shift (B) or peak intensity changes (C) over time after the addition of CD for various DOPC resonances in the presence or absence of MscS at 2:1 CD-to-lipid ratio. Dots represent the experimental data and solid lines single exponential fits, resonance t (blue), m (green) in the context of empty NDs (open symbols) or loaded (+MscS) NDs (filled symbols). The calculated rates from fits to the ^{1}H chemical shift or intensity changes are shown as bars in D. The errors were calculated from the covariance matrix that is generated from the single exponential fit to the experimental data.

Nevertheless, the trends in the primary data for both MscS reporters reproduce the *in silico* predictions for conformational changes in a small fraction of channels (Figures 2 and S3). Therefore, the two most obvious lessons are that these changes can be traced in an ensemble of MscS channels and that EPR is a method to detect this, even if only a few percent in an ensemble change conformation.

Monitoring lipid movement under molecular tension by NMR spectroscopy

In order to link lipid motions to MscS changes monitored by PELDOR and electrophysiology, we next probed lipid movement, under molecular tension by NMR. Under prolonged CD incubation, NDs reduce their lipid density and eventually lose their structural integrity and aggregate. However, it is unknown whether the channel's presence affects the lipid depletion rate, which is linked to the kinetics of molecular tension generation. Monitoring CD-induced lipid (including different domains within the lipid) depletion that proceeds in parallel with ND aggregation and quantifying such a process is a challenging task, which we addressed by employing real-time NMR spectroscopy. CD was added to the NMR sample and was present for the duration of the NMR experiments, as was done in patch-clamp electrophysiology experiments which differed only in the lipid scaffold used (NDs vs. GUVs). For consistency with our PELDOR, NMR experiments were carried out using functional MscS D67R1 channels reconstituted in DOPC NDs. ^{1}H–^{13}C SOFAST-HMQC spectra were recorded in real time, following the addition of CD at the same ratio and lipid composition as the one used for PELDOR and similar ratios and lipids (i.e., DOPC) to the ones used to capture activated MscS by cryo-EM in NDs.[14] Signals corresponding to different parts of the DOPC molecules are observed, even at natural abundance, owing to the large number of lipids present in the sample (Figures 3A and S4A). NMR chemical shifts are highly sensitive reporters of the local electronic environment and could therefore probe the transition of a lipid from being embedded in an ND to being bound to CD. On the other hand, a uniform across all resonances, time-dependent reduction in NMR peak intensities is a characteristic hallmark of aggregation.[64] To test the effect of CD, we first incubated empty DOPC NDs with CD at different CD-to-lipid ratios and collected ^{1}H–^{13}C SOFAST-HMQC spectra in real time at 2:1 CD-to-lipid ratio (Figure 3). ^{13}C chemical shifts were largely unaffected (Figure S4); however, ^{1}H shifts gradually reduced their values over time. The rate of chemical shift change was similar for all DOPC resonances and was dependent on the CD-to-lipid ratio (2:1, 6:1, 12:1) used (Figures S4 and S5), further supporting the notion that ^{1}H shifts report on CD-induced lipid depletion. Note that despite the differences in lipid depletion rates, the final ppm equilibrium that was reached for all the CD-to-lipid ratios used was the same. This indicates that after initial CD interactions with ND lipids, the latter become inaccessible to CD. On the other hand, the rate of loss of NMR intensities over time was not affected by increasing the CD-to-lipid ratio (Figure S5), a fact that could suggest that lipid depletion and ND aggregation proceed through distinct pathways, hinting the presence of different molecular mechanisms. NMR intensities seem to plateau at ~50% of their initial value after ~12 h suggesting that half of the NDs in solution preserve their structural integrity and withstand aggregation even after prolonged CD incubation. Chemical shifts also reach a plateau after ~240 min, indicative of the establishment of a new equilibrium. We then performed the same real-time NMR experiments at 2:1 CD-to-lipid ratio, using

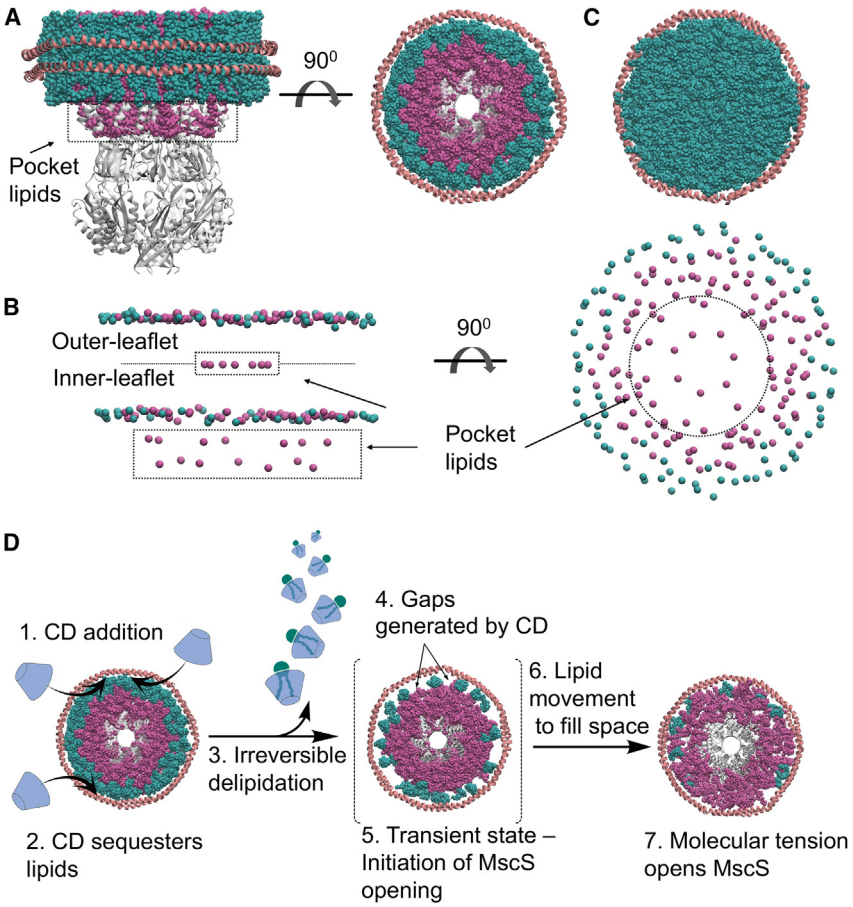

Figure 4. Model for the generation of CD-induced molecular tension and the activation of MscS

(A) Charmm-gui[65] representation of MscS reconstituted in NDs, in agreement with molecular dynamic simulations on and structures of MscS.[9,69] 130 lipids are within 15 Å of MscS (MscS-interacting lipids, mauve spheres) and the remaining 90 lipids (bulk bilayer, cyan spheres). Belt proteins (MSP1D1E3) and MscS are represented as cartoons, in pink and gray, respectively (side and top periplasmic views).

(B) As in (A), but MscS and belt proteins are not depicted for clarity. DOPC lipids are represented by their P head group atoms (side and top views). ~21 pocket lipids, which according to the lipid-moves-first model[6,9] act as negative allosteric modulators for MscS, are indicated with arrows (side and top views). (C) Top view of ND filled with lipids (empty NDs – devoid of MscS) composed of bulk lipids (274 in total, outer- and inner-leaflet, cyan spheres).

(D) Model of molecular tension. 1. CD is added to NDs loaded with MscS (gray cartoon). MscS initially adopts a closed conformation. 2. CD first sequesters the bulk lipids, which are located mostly in the ND periphery and are depleted two orders of magnitude faster than the MscS-interacting lipids. 3. CD causes irreversible delipidation as depleted lipids are permanently removed. 4. This generates gaps within the ND and a short-lived transient state during which MscS opening is initiated (5). 6. Remaining lipids, which in their majority consist of MscS-interacting lipids move to fill these gaps. 7. This lipid movement induces a membrane tension build-up, creating conditions of molecular tension, which activate MscS (open state, PDB: 5AJI[9]).

MscS D67R1-loaded DOPC NDs under the same conditions. Although the rate of signal loss was largely the same in comparison to that of empty NDs at the same CD-to-lipid ratio (~0.0063/0.0076 min^{-1} respectively), the rate of chemical shift changes has drastically slowed down for resonances arising from both the middle and end of the acyl chain (0.0017/0.0009 min^{-1}, respectively) (Figure 3). As judged by the ^{1}H shifts at the end of the reaction, the final equilibrium reached following prolonged incubation with CD is similar in both empty and NDs loaded with MscS. Indeed, we found the equilibrium is reached approximately 7× times slower in the presence of MscS. We note that in MscS' presence, the CD-to-lipid ratio we quote is likely an underestimation, as MscS is expected to displace a substantial number of lipids when mixed with NDs. Therefore, lipid depletion of the bulk ND lipids is expected to occur even faster than the rates we measured by NMR.

We then calculated the loss in the number of lipids being displaced by MscS during reconstitution. We assembled (using the Charmm-gui[65] membrane builder tool[66]) empty (i.e., devoid of MscS) MSP1D1E3 NDs with DOPC lipids (Figure 4C), and found that these contain a total of 274 DOPC lipids, i.e., 137 inner- and 137 outer-leaflet. We then assembled the same NDs loaded with MscS, which now contained a total of 220 DOPC lipids, i.e., 94 inner- and 113 outer-leaflet (Figure 4A). This comparison suggests that MscS displaces approximately 54 DOPC lipids (asymmetrically between the two leaflets) upon reconstitution, which accounts for ~20% of the initial ND lipid population. Therefore, even 20% faster depletion rates occur in empty, compared to NDs loaded with MscS. This is remarkable given that upon reconstitution the lipid population is reduced, and one would expect MscS' presence to accelerate rather than slow down lipid depletion rates. Nevertheless, these differences may well explain the time differences observed in MscS activation, when NDs (PELDOR or cryo-EM) or GUVs (electrophysiology) are used.

DISCUSSION

Prolonged openings of MscS under sustained tension would lead to cell toxicity. To avoid irreversible effects and ensure cell survival under stress conditions, MscS becomes temporarily insensitive to membrane tension. After we recorded single-channel activities for a wide range of CD-to-lipid ratios, tension reapplication led to either membrane rupture (n = 14) or channel inactivity (n = 13), suggesting MscS enters a desensitized (or inactivated)[16] state, similar to the effect conferred by naturally applied tension. This included cases in which no MscS activation following CD incubation was observed. Such irreversible channel behavior, though, is in contrast to naturally occurring tension-induced desensitization, where channels are able to return to a closed state after a short period of inactivity.[67]

Our real-time NMR showed the same equilibrium was reached independent of the CD-to-lipid ratio used. The higher the

CD-to-lipid ratio, the faster the depletion rate, but we recorded no increase between 6:1 and 12:1 ratio. These observations are consistent with CD interacting with lipids and irreversibly altering their state in a way that lipids become inaccessible and cannot be sequestered by CD anymore. The difference between CD-induced and naturally occurring tension is that in the latter case, there is lipid availability to allow MscS closure, in contrast to the former case where lipids are permanently removed from membranes. Our observations lend further support to the entropy-driven lipid-moves-first model according to which there must be lipid re-availability in the vicinity of MscS' inner-leaflet pockets, for lipids to re-enter, apply pressure to the gate, and close the channel.[6,9] The range of the observed states and the timing of their activation varies when different CD-to-lipid ratios are used. MscS openings lasted for up to several hours until desensitization dominated the active channel population within our patches. This is consistent with previous studies where the extent of lipid availability within pockets led to distinct conducting states in MscS, with pocket lipid density being the lowest in the desensitized, compared to closed, open, and sub-conducting states.[14,16,17]

Here, we specifically included the same order of magnitude CD-to-lipid ratio in both our ensemble (12:1) and single-channel experiments (20:1) to link structural changes (PELDOR) and lipid movement (NMR) to the functional behavior (electrophysiology) of MscS. Our combination of ensemble and single-molecule methods yields a consistent picture which shows that CD leads to structural rearrangements in MscS and lipid depletion is reproduced in all three kinds of experiments, though observed at different time scales (i.e., hours in PELDOR/NMR vs. minutes in electrophysiology). Our PELDOR experiments show unambiguous conformational changes, toward MscS opening(s), given that all intermediate S1-S5 sub-conducting states would give rise to distances that are in-between the C and FO states. Single-channel recordings at similar CD-to-lipid ratios resulted in sub-openings followed by desensitization, which was only observed after a few hours of CD addition. Notably, to form GUVs, we used a much lower MscS to lipid (1–6000) ratio than the one we used for reconstitution in NDs for PELDOR (1–31). This made the presence of MscS within our GUV excised membrane patches of $\sim 3 \times 10^6$ nm^2 area (glass pipette diameter of ~ 2 μm) very rare, with a maximum of 30× active MscS channels we were able to detect within a single patch. This number of MscS channels could occupy $\sim 1.5 \times 10^2$ nm^2, accounting for 0.05% of the total membrane patch area. Therefore, diluted MscS has a negligible effect in slowing down lipid depletion from the GUV patches and depletion is expected with similar rates as measured for empty, rather than dense NDs loaded with MscS. In PELDOR, all processes were thus delayed by at least an order of magnitude (as in previous cryo-EM studies[14]), with MscS opening(s) occurring within hours of CD incubation, compared to minutes in electrophysiology.

Due to the small PELDOR model distance differences and the lack of available MscS sub-conducting state structures (only one has been reported to date), we could not discriminate between the resolved sub-conducting state (PDB 6VYL),[14] with a ~10 Å pore diameter and predicted conductance of 600–800 pS,[68] consistent to the intermediate S1 or S2 state (Figure S6) and the other MscS intermediates (S3-S5). Our PELDOR data are consistent with sub-openings based on model distances for the FO and the resolved sub-conducting state. Notably, for increasing CD-to-lipid ratios, we obtained different ranges of sub-conducting states, with higher conductance states (FO, S1-S3) only appearing at the highest CD-to-lipid ratios (30,000:1) (Figures 1 and S2). These MscS state ensembles generated by CD-induced membrane tension are not sufficiently monodisperse to enable high-resolution structure determination for neither the FO, nor the S1 (or S2) state. Indeed, structure acquisition of the latter was only made possible by using thinner PC:10 bilayers to force a single monodisperse MscS substate[14] (i.e., S1 or S2, Figure S6). However, longer incubation times with CD and higher ratios led to a desensitized state, which dominated the MscS conformational state ensemble (consistent with our observations in electrophysiology), enabling structure acquisition by cryo-EM. It is quite intriguing that a range of sub-conducting openings appeared under the same CD-to-lipid ratios, suggesting that molecular tension has a differential effect on individual channels. Channel opening events in electrophysiology could occur in the presence of closed, desensitized, and/or other non-conducting channels while in PELDOR and NMR the entire ensemble of channels (and their states) is monitored. The number of openings within our ensemble did not increase following longer incubation times under same ratios and a slightly higher number of openings were observed for higher 6:1 and 12:1 ratio and 16 h of CD incubation. However, high-resolution structures for each one of these intermediate states are required to verify this. A similar ratio (20:1) was used in our single-channel recordings with MscS opening to low sub-conducting state(s) (S3-S5) of its tension-mediated pathway. A low sub-conducting state was shown to be crucial in the gating of the structurally diverse MS channel of large conductance MscL, obtained by either applying tension or disrupting lipid access to TM pockets.[20–23]

Lipid disengagement from NDs by CD was dependent on MscS' presence and although changes after 4 h continued to occur, these were small, due to MscS dramatically slowing this process down. This is surprising since one would expect that depletion would be faster for a lower amount of lipids, given that MscS displaces ~20% of ND lipids upon reconstitution (Figures 3 and 4). The hypothesis of MscS-interacting lipids (including the pocket lipids) being spatially restricted for CD to access and sequester is consistent with our NMR findings in which lipids become inaccessible to CD after initial interaction. In contrast, bulk bilayer lipids should be readily accessible to CD and mostly reside within the periphery of NDs loaded with MscS (Figures 4A–4C). A plausible model that could explain the observed data is that bulk lipids are depleted much faster than the MscS-interacting lipids (Figure 4D). We calculated that from the initial 274 DOPC bulk lipids of an "empty" MSP1D1E3 ND, 130 lipids interact with MscS. Within these MscS-interacting lipids, approximately half are annular lipids, forming tighter interactions with MscS. This number is consistent with a MscS structure in complex with 63 (9 per MscS subunit) lipid-like molecules,[16] one-third of which form the cytoplasmic-leaflet pocket lipids, crucial to MscS' gating (Figures 4A and 4B). With 54 ND lipids being displaced by MscS during reconstitution, the remaining 90 lipids do not interact with MscS (termed as bulk lipids, Figures 4A–4C). The depletion rate is dependent

on lipid availability and CD accessibility and these in turn depend on the ND size (determined by the MSP belt-protein length), the lipid composition (CD has differential lipid head group preference[15]), and the reconstituted membrane protein cross-sectional area (with respect to ND size).

So far, MscS structures solved by either X-ray crystallography or cryo-EM have been reported for the C, DS (or IC), FO, and a sub-conducting state bearing properties consistent with the S1 or S2 state. Yet at least four sub- and a non-conducting state(s) have not been characterized, hindering efforts to elucidate the gating mechanism of MscS. By varying the CD-to-lipid ratio, we hereby identified molecular conditions for accessing distinct functional MscS sub-state(s) and showed that PELDOR can detect minute changes within its conformational ensemble, complemented by the NMR-informed associated lipid motions, which occur under molecular tension.

STAR★METHODS

Detailed methods are provided in the online version of this paper and include the following:

- KEY RESOURCES TABLE
- RESOURCE AVAILABILITY
  - Lead contact
  - Material availability
  - Data and code availability
- EXPERIMENTAL MODEL AND STUDY PARTICIPANT DETAILS
- METHOD DETAILS
  - Expression, purification, and spin labeling of MscS
  - MscS reconstitution into nanodics
  - Treatment of MscS-containing NDs with CD
  - PELDOR (or DEER) spectroscopy
  - Sample preparation for NMR spectroscopy
  - NMR spectroscopy
  - MscS reconstitution into proteoliposomes
  - GUVs formation and electrophysiology
  - Treatment of MscS-containing GUVs with CD
- QUANTIFICATION AND STATISTICAL ANALYSIS

SUPPLEMENTAL INFORMATION

Supplemental information can be found online at https://doi.org/10.1016/j.str.2024.02.020.

ACKNOWLEDGMENTS

This project was supported by a Biotechnology and Biological Sciences Research Council (BBSRC) grant (BB/S018069/1) to C.P., who acknowledges support from the Wellcome Trust (WT) (219999/Z/19/Z) in the form of studentship for B.J.L. We also acknowledge support from the Chinese Scholarship Council (CSC) in the form of studentships for N.Y., Y.M., B.W., respectively. T.K.K. is supported by a Sir Henry Dale Fellowship funded by the WT and the Royal Society (223268/Z/21/Z). B.E.B. and C.P. thank the Leverhulme Trust (RPG-2018-397) for support. Funding from BBSRC (BB/R013780/1; BB/T017740/1) equipment grants enabled the purchase of the Qband Bruker pulse EPR spectrometer and University of Leeds funding the Bruker 950 MHz NMR spectrometer. The authors would like to thank Dr. Jonathan Lippiat for help with the electrophysiology setup.

AUTHOR CONTRIBUTIONS

C.P. conceived and designed the project with help from T.K.K. and B.E.B. B.J.L., Y.M., N.Y., B.W., and K.A. performed the research. All authors processed and analyzed the data. C.P. wrote the manuscript, assisted by B.J.L., T.K.K., and B.E.B. All authors provided critical feedback and helped shape the research, analysis, and manuscript.

DECLARATION OF INTERESTS

The authors declare no competing interests.

Received: September 14, 2023
Revised: December 29, 2023
Accepted: February 27, 2024
Published: March 22, 2024

REFERENCES

1. Booth, I.R., and Blount, P. (2012). The MscS and MscL families of mechanosensitive channels act as microbial emergency release valves. J. Bacteriol. *194*, 4802–4809. https://doi.org/10.1128/JB.00576-12.
2. Kung, C., Martinac, B., and Sukharev, S. (2010). Mechanosensitive channels in microbes. Annu. Rev. Microbiol. *64*, 313–329. https://doi.org/10.1146/annurev.micro.112408.134106.
3. Booth, I.R., Edwards, M.D., Black, S., Schumann, U., and Miller, S. (2007). Mechanosensitive channels in bacteria: signs of closure? Nat. Rev. Microbiol. *5*, 431–440. https://doi.org/10.1038/nrmicro1659.
4. Levina, N., Tötemeyer, S., Stokes, N.R., Louis, P., Jones, M.A., and Booth, I.R. (1999). Protection of Escherichia coli cells against extreme turgor by activation of MscS and MscL mechanosensitive channels: identification of genes required for MscS activity. EMBO J. *18*, 1730–1737.
5. Cox, C.D., Nakayama, Y., Nomura, T., and Martinac, B. (2015). The evolutionary 'tinkering' of MscS-like channels: generation of structural and functional diversity. Pflugers Arch. *467*, 3–13. https://doi.org/10.1007/s00424-014-1522-2.
6. Pliotas, C., and Naismith, J.H. (2017). Spectator no more, the role of the membrane in regulating ion channel function. Curr. Opin. Struct. Biol. *45*, 59–66. https://doi.org/10.1016/j.sbi.2016.10.017.
7. Teng, J., Loukin, S., Anishkin, A., and Kung, C. (2015). The force-from-lipid (FFL) principle of mechanosensitivity, at large and in elements. Pflugers Arch. *467*, 27–37. https://doi.org/10.1007/s00424-014-1530-2.
8. Nomura, T., Cranfield, C.G., Deplazes, E., Owen, D.M., Macmillan, A., Battle, A.R., Constantine, M., Sokabe, M., and Martinac, B. (2012). Differential effects of lipids and lyso-lipids on the mechanosensitivity of the mechanosensitive channels MscL and MscS. Proc. Natl. Acad. Sci. USA *109*, 8770–8775. https://doi.org/10.1073/pnas.1200051109.
9. Pliotas, C., Dahl, A.C.E., Rasmussen, T., Mahendran, K.R., Smith, T.K., Marius, P., Gault, J., Banda, T., Rasmussen, A., Miller, S., et al. (2015). The role of lipids in mechanosensation. Nat. Struct. Mol. Biol. *22*, 991–998. https://doi.org/10.1038/nsmb.3120.
10. Kefauver, J.M., Ward, A.B., and Patapoutian, A. (2020). Discoveries in structure and physiology of mechanically activated ion channels. Nature *587*, 567–576. https://doi.org/10.1038/s41586-020-2933-1.
11. Malcolm, H.R., Blount, P., and Maurer, J.A. (2015). The mechanosensitive channel of small conductance (MscS) functions as a Jack-in-the box. Biochim. Biophys. Acta *1848*, 159–166. https://doi.org/10.1016/j.bbamem.2014.10.022.
12. Haswell, E.S., Phillips, R., and Rees, D.C. (2011). Mechanosensitive channels: what can they do and how do they do it? Structure *19*, 1356–1369. https://doi.org/10.1016/j.str.2011.09.005.
13. Naismith, J.H., and Booth, I.R. (2012). Bacterial mechanosensitive channels–MscS: evolution's solution to creating sensitivity in function. Annu. Rev. Biophys. *41*, 157–177. https://doi.org/10.1146/annurev-biophys-101211-113227.

14. Zhang, Y., Daday, C., Gu, R.X., Cox, C.D., Martinac, B., de Groot, B.L., and Walz, T. (2021). Visualization of the mechanosensitive ion channel MscS under membrane tension. Nature *590*, 509–514. https://doi.org/10.1038/s41586-021-03196-w.

15. Cox, C.D., Zhang, Y., Zhou, Z., Walz, T., and Martinac, B. (2021). Cyclodextrins increase membrane tension and are universal activators of mechanosensitive channels. Proc. Natl. Acad. Sci. USA *118*, e2104820118. https://doi.org/10.1073/pnas.2104820118.

16. Flegler, V.J., Rasmussen, A., Borbil, K., Boten, L., Chen, H.A., Deinlein, H., Halang, J., Hellmanzik, K., Löffler, J., Schmidt, V., et al. (2021). Mechanosensitive channel gating by delipidation. Proc. Natl. Acad. Sci. USA *118*, e2107095118. https://doi.org/10.1073/pnas.2107095118.

17. Reddy, B., Bavi, N., Lu, A., Park, Y., and Perozo, E. (2019). Molecular basis of force-from-lipids gating in the mechanosensitive channel MscS. Elife *8*, e50486. https://doi.org/10.7554/eLife.50486.

18. Wang, W., Black, S.S., Edwards, M.D., Miller, S., Morrison, E.L., Bartlett, W., Dong, C., Naismith, J.H., and Booth, I.R. (2008). The structure of an open form of an E. coli mechanosensitive channel at 3.45 A resolution. Science *321*, 1179–1183. https://doi.org/10.1126/science.1159262.

19. Bass, R.B., Strop, P., Barclay, M., and Rees, D.C. (2002). Crystal structure of Escherichia coli MscS, a voltage-modulated and mechanosensitive channel. Science *298*, 1582–1587. https://doi.org/10.1126/science.1077945.

20. Wang, B., Lane, B.J., Kapsalis, C., Ault, J.R., Sobott, F., El Mkami, H., Calabrese, A.N., Kalli, A.C., and Pliotas, C. (2022). Pocket delipidation induced by membrane tension or modification leads to a structurally analogous mechanosensitive channel state. Structure *30*, 608–622.e5. https://doi.org/10.1016/j.str.2021.12.004.

21. Kapsalis, C., Wang, B., El Mkami, H., Pitt, S.J., Schnell, J.R., Smith, T.K., Lippiat, J.D., Bode, B.E., and Pliotas, C. (2019). Allosteric activation of an ion channel triggered by modification of mechanosensitive nano-pockets. Nat. Commun. *10*, 4619. https://doi.org/10.1038/s41467-019-12591-x.

22. Chiang, C.S., Anishkin, A., and Sukharev, S. (2004). Gating of the large mechanosensitive channel in situ: estimation of the spatial scale of the transition from channel population responses. Biophys. J. *86*, 2846–2861. https://doi.org/10.1016/s0006-3495(04)74337-4.

23. Sukharev, S., Betanzos, M., Chiang, C.S., and Guy, H.R. (2001). The gating mechanism of the large mechanosensitive channel MscL. Nature *409*, 720–724. https://doi.org/10.1038/35055559.

24. Kapsalis, C., Ma, Y., Bode, B.E., and Pliotas, C. (2020). In-Lipid Structure of Pressure-Sensitive Domains Hints Mechanosensitive Channel Functional Diversity. Biophys. J. *119*, 448–459. https://doi.org/10.1016/j.bpj.2020.06.012.

25. Dionysopoulou, M., Yan, N., Wang, B., Pliotas, C., and Diallinas, G. (2022). Genetic and cellular characterization of MscS-like putative channels in the filamentous fungus Aspergillus nidulans. Channels *16*, 148–158. https://doi.org/10.1080/19336950.2022.2098661.

26. Deng, Z., Maksaev, G., Schlegel, A.M., Zhang, J., Rau, M., Fitzpatrick, J.A.J., Haswell, E.S., and Yuan, P. (2020). Structural mechanism for gating of a eukaryotic mechanosensitive channel of small conductance. Nat. Commun. *11*, 3690. https://doi.org/10.1038/s41467-020-17538-1.

27. Maksaev, G., and Haswell, E.S. (2012). MscS-Like10 is a stretch-activated ion channel from Arabidopsis thaliana with a preference for anions. Proc. Natl. Acad. Sci. USA *109*, 19015–19020. https://doi.org/10.1073/pnas.1213931109.

28. Mount, J., Maksaev, G., Summers, B.T., Fitzpatrick, J.A.J., and Yuan, P. (2022). Structural basis for mechanotransduction in a potassium-dependent mechanosensitive ion channel. Nat. Commun. *13*, 6904. https://doi.org/10.1038/s41467-022-34737-0.

29. Edwards, M.D., Black, S., Rasmussen, T., Rasmussen, A., Stokes, N.R., Stephen, T.L., Miller, S., and Booth, I.R. (2012). Characterization of three novel mechanosensitive channel activities in Escherichia coli. Channels *6*, 272–281. https://doi.org/10.4161/chan.20998.

30. Schumann, U., Edwards, M.D., Rasmussen, T., Bartlett, W., van West, P., and Booth, I.R. (2010). YbdG in Escherichia coli is a threshold-setting mechanosensitive channel with MscM activity. Proc. Natl. Acad. Sci. USA *107*, 12664–12669. https://doi.org/10.1073/pnas.1001405107.

31. Li, Y., Moe, P.C., Chandrasekaran, S., Booth, I.R., and Blount, P. (2002). Ionic regulation of MscK, a mechanosensitive channel from Escherichia coli. EMBO J. *21*, 5323–5330. https://doi.org/10.1093/emboj/cdf537.

32. Flegler, V.J., Rasmussen, A., Rao, S., Wu, N., Zenobi, R., Sansom, M.S.P., Hedrich, R., Rasmussen, T., and Böttcher, B. (2020). The MscS-like channel Ynal has a gating mechanism based on flexible pore helices. Proc. Natl. Acad. Sci. USA *117*, 28754–28762. https://doi.org/10.1073/pnas.2005641117.

33. Jojoa-Cruz, S., Saotome, K., Tsui, C.C.A., Lee, W.H., Sansom, M.S.P., Murthy, S.E., Patapoutian, A., and Ward, A.B. (2022). Structural insights into the Venus flytrap mechanosensitive ion channel Flycatcher1. Nat. Commun. *13*, 850. https://doi.org/10.1038/s41467-022-28511-5.

34. Ward, R., Pliotas, C., Branigan, E., Hacker, C., Rasmussen, A., Hagelueken, G., Booth, I.R., Miller, S., Lucocq, J., Naismith, J.H., and Schiemann, O. (2014). Probing the structure of the mechanosensitive channel of small conductance in lipid bilayers with pulsed electron-electron double resonance. Biophys. J. *106*, 834–842. https://doi.org/10.1016/j.bpj.2014.01.008.

35. Pliotas, C., Ward, R., Branigan, E., Rasmussen, A., Hagelueken, G., Huang, H., Black, S.S., Booth, I.R., Schiemann, O., and Naismith, J.H. (2012). Conformational state of the MscS mechanosensitive channel in solution revealed by pulsed electron-electron double resonance (PELDOR) spectroscopy. Proc. Natl. Acad. Sci. USA *109*, E2675–E2682. https://doi.org/10.1073/pnas.1202286109.

36. Brohawn, S.G., Campbell, E.B., and MacKinnon, R. (2014). Physical mechanism for gating and mechanosensitivity of the human TRAAK K+ channel. Nature *516*, 126–130. https://doi.org/10.1038/nature14013.

37. Rasmussen, T., Flegler, V.J., Rasmussen, A., and Böttcher, B. (2019). Structure of the Mechanosensitive Channel MscS Embedded in the Membrane Bilayer. J. Mol. Biol. *431*, 3081–3090. https://doi.org/10.1016/j.jmb.2019.07.006.

38. Rasmussen, T., Rasmussen, A., Yang, L., Kaul, C., Black, S., Galbiati, H., Conway, S.J., Miller, S., Blount, P., and Booth, I.R. (2019). Interaction of the Mechanosensitive Channel, MscS, with the Membrane Bilayer through Lipid Intercalation into Grooves and Pockets. J. Mol. Biol. *431*, 3339–3352. https://doi.org/10.1016/j.jmb.2019.05.043.

39. Tsamaloukas, A., Szadkowska, H., Slotte, P.J., and Heerklotz, H. (2005). Interactions of cholesterol with lipid membranes and cyclodextrin characterized by calorimetry. Biophys. J. *89*, 1109–1119. https://doi.org/10.1529/biophysj.105.061846.

40. López, C.A., de Vries, A.H., and Marrink, S.J. (2011). Molecular mechanism of cyclodextrin mediated cholesterol extraction. PLoS Comput. Biol. *7*, e1002020. https://doi.org/10.1371/journal.pcbi.1002020.

41. Hofmann, L., and Ruthstein, S. (2022). EPR Spectroscopy Provides New Insights into Complex Biological Reaction Mechanisms. J. Phys. Chem. B *126*, 7486–7494. https://doi.org/10.1021/acs.jpcb.2c05235.

42. Jeschke, G. (2012). DEER distance measurements on proteins. Annu. Rev. Phys. Chem. *63*, 419–446. https://doi.org/10.1146/annurev-physchem-032511-143716.

43. Hustedt, E.J., Stein, R.A., and McHaourab, H.S. (2021). Protein functional dynamics from the rigorous global analysis of DEER data: Conditions, components, and conformations. J. Gen. Physiol. *153*, e201711954. https://doi.org/10.1085/jgp.201711954.

44. Galazzo, L., Teucher, M., and Bordignon, E. (2022). Orthogonal spin labeling and pulsed dipolar spectroscopy for protein studies. Methods Enzymol. *666*, 79–119. https://doi.org/10.1016/bs.mie.2022.02.004.

45. Haysom, S.F., Machin, J., Whitehouse, J.M., Horne, J.E., Fenn, K., Ma, Y., El Mkami, H., Böhringer, N., Schäberle, T.F., Ranson, N.A., et al. (2023). Darobactin B Stabilises a Lateral-Closed Conformation of the BAM Complex in E. coli Cells. Angew. Chem. Int. Ed. Engl. *62*, e202218783. https://doi.org/10.1002/anie.202218783.

46. Ketter, S., and Joseph, B. (2023). Gd(3+)-Trityl-Nitroxide Triple Labeling and Distance Measurements in the Heterooligomeric Cobalamin Transport Complex in the Native Lipid Bilayers. J. Am. Chem. Soc. *145*, 960–966. https://doi.org/10.1021/jacs.2c10080.

47. Wingler, L.M., Elgeti, M., Hilger, D., Latorraca, N.R., Lerch, M.T., Staus, D.P., Dror, R.O., Kobilka, B.K., Hubbell, W.L., and Lefkowitz, R.J. (2019). Angiotensin Analogs with Divergent Bias Stabilize Distinct Receptor Conformations. Cell *176*, 468–478.e11. https://doi.org/10.1016/j.cell.2018.12.005.

48. Kubatova, N., Schmidt, T., Schwieters, C.D., and Clore, G.M. (2023). Quantitative analysis of sterol-modulated monomer-dimer equilibrium of the beta(1)-adrenergic receptor by DEER spectroscopy. Proc. Natl. Acad. Sci. USA *120*, e2221036120. https://doi.org/10.1073/pnas.2221036120.

49. Bountra, K., Hagelueken, G., Choudhury, H.G., Corradi, V., El Omari, K., Wagner, A., Mathavan, I., Zirah, S., Yuan Wahlgren, W., Tieleman, D.P., et al. (2017). Structural basis for antibacterial peptide self-immunity by the bacterial ABC transporter McjD. EMBO J. *36*, 3062–3079. https://doi.org/10.15252/embj.201797278.

50. Hartley, A.M., Ma, Y., Lane, B.J., Wang, B., and Pliotas, C. (2020). Using pulsed EPR in the structural analysis of integral membrane proteins. Electron Paramagn. Reson. *27*, 74–108.

51. Pliotas, C. (2017). Ion Channel Conformation and Oligomerization Assessment by Site-Directed Spin Labeling and Pulsed-EPR. Methods Enzymol. *594*, 203–242. https://doi.org/10.1016/bs.mie.2017.05.013.

52. Frei, J.N., Broadhurst, R.W., Bostock, M.J., Solt, A., Jones, A.J.Y., Gabriel, F., Tandale, A., Shrestha, B., and Nietlispach, D. (2020). Conformational plasticity of ligand-bound and ternary GPCR complexes studied by (19)F NMR of the beta(1)-adrenergic receptor. Nat. Commun. *11*, 669. https://doi.org/10.1038/s41467-020-14526-3.

53. Bostock, M.J., Solt, A.S., and Nietlispach, D. (2019). The role of NMR spectroscopy in mapping the conformational landscape of GPCRs. Curr. Opin. Struct. Biol. *57*, 145–156. https://doi.org/10.1016/j.sbi.2019.03.030.

54. Shukla, R., Lavore, F., Maity, S., Derks, M.G.N., Jones, C.R., Vermeulen, B.J.A., Melcrová, A., Morris, M.A., Becker, L.M., Wang, X., et al. (2022). Teixobactin kills bacteria by a two-pronged attack on the cell envelope. Nature *608*, 390–396. https://doi.org/10.1038/s41586-022-05019-y.

55. Goretzki, B., Guhl, C., Tebbe, F., Harder, J.M., and Hellmich, U.A. (2021). Unstructural Biology of TRP Ion Channels: The Role of Intrinsically Disordered Regions in Channel Function and Regulation. J. Mol. Biol. *433*, 166931. https://doi.org/10.1016/j.jmb.2021.166931.

56. Battle, A.R., Petrov, E., Pal, P., and Martinac, B. (2009). Rapid and improved reconstitution of bacterial mechanosensitive ion channel proteins MscS and MscL into liposomes using a modified sucrose method. FEBS Lett. *583*, 407–412. https://doi.org/10.1016/j.febslet.2008.12.033.

57. Martinac, B., Buechner, M., Delcour, A.H., Adler, J., and Kung, C. (1987). Pressure-sensitive ion channel in Escherichia coli. Proc. Natl. Acad. Sci. USA *84*, 2297–2301. https://doi.org/10.1073/pnas.84.8.2297.

58. Opsahl, L.R., and Webb, W.W. (1994). Lipid-glass adhesion in giga-sealed patch-clamped membranes. Biophys. J. *66*, 75–79. https://doi.org/10.1016/s0006-3495(94)80752-0.

59. Denisov, I.G., Grinkova, Y.V., Lazarides, A.A., and Sligar, S.G. (2004). Directed self-assembly of monodisperse phospholipid bilayer Nanodiscs with controlled size. J. Am. Chem. Soc. *126*, 3477–3487. https://doi.org/10.1021/ja0393574.

60. Sukharev, S. (2002). Purification of the small mechanosensitive channel of Escherichia coli (MscS): the subunit structure, conduction, and gating characteristics in liposomes. Biophys. J. *83*, 290–298. https://doi.org/10.1016/S0006-3495(02)75169-2.

61. Ackermann, K., Pliotas, C., Valera, S., Naismith, J.H., and Bode, B.E. (2017). Sparse Labeling PELDOR Spectroscopy on Multimeric Mechanosensitive Membrane Channels. Biophys. J. *113*, 1968–1978. https://doi.org/10.1016/j.bpj.2017.09.005.

62. Valera, S., Ackermann, K., Pliotas, C., Huang, H., Naismith, J.H., and Bode, B.E. (2016). Accurate Extraction of Nanometer Distances in Multimers by Pulse EPR. Chemistry (Weinheim an der Bergstrasse, Germany) *22*, 4700–4703. https://doi.org/10.1002/chem.201505143.

63. McQuarrie, S., Athukoralage, J.S., McMahon, S.A., Graham, S., Ackermann, K., Bode, B.E., White, M.F., and Gloster, T.M. (2023). Activation of Csm6 ribonuclease by cyclic nucleotide binding: in an emergency, twist to open. Nucleic Acids Res. *51*, 10590–10605. https://doi.org/10.1093/nar/gkad739.

64. Karamanos, T.K., Kalverda, A.P., Thompson, G.S., and Radford, S.E. (2015). Mechanisms of amyloid formation revealed by solution NMR. Prog. Nucl. Magn. Reson. Spectrosc. *88–89*, 86–104. https://doi.org/10.1016/j.pnmrs.2015.05.002.

65. Jo, S., Kim, T., Iyer, V.G., and Im, W. (2008). CHARMM-GUI: a web-based graphical user interface for CHARMM. J. Comput. Chem. *29*, 1859–1865. https://doi.org/10.1002/jcc.20945.

66. Jo, S., Lim, J.B., Klauda, J.B., and Im, W. (2009). CHARMM-GUI Membrane Builder for mixed bilayers and its application to yeast membranes. Biophys. J. *97*, 50–58. https://doi.org/10.1016/j.bpj.2009.04.013.

67. Kamaraju, K., Belyy, V., Rowe, I., Anishkin, A., and Sukharev, S. (2011). The pathway and spatial scale for MscS inactivation. J. Gen. Physiol. *138*, 49–57. https://doi.org/10.1085/jgp.201110606.

68. Cruickshank, C.C., Minchin, R.F., Le Dain, A.C., and Martinac, B. (1997). Estimation of the pore size of the large-conductance mechanosensitive ion channel of Escherichia coli. Biophys. J. *73*, 1925–1931. https://doi.org/10.1016/s0006-3495(97)78223-7.

69. Park, Y.C., Reddy, B., Bavi, N., Perozo, E., and Faraldo-Gómez, J.D. (2023). State-specific morphological deformations of the lipid bilayer explain mechanosensitive gating of MscS ion channels. Elife *12*, e81445. https://doi.org/10.7554/eLife.81445.

70. Lane, B.J., Wang, B., Ma, Y., Calabrese, A.N., El Mkami, H., and Pliotas, C. (2022). HDX-guided EPR spectroscopy to interrogate membrane protein dynamics. STAR Protoc. *3*, 101562. https://doi.org/10.1016/j.xpro.2022.101562.

71. Branigan, E., Pliotas, C., Hagelueken, G., and Naismith, J.H. (2013). Quantification of free cysteines in membrane and soluble proteins using a fluorescent dye and thermal unfolding. Nat. Protoc. *8*, 2090–2097. https://doi.org/10.1038/nprot.2013.128.

72. Michou, M., Kapsalis, C., Pliotas, C., and Skretas, G. (2019). Optimization of Recombinant Membrane Protein Production in the Engineered Escherichia coli Strains SuptoxD and SuptoxR. ACS Synth. Biol. *8*, 1631–1641. https://doi.org/10.1021/acssynbio.9b00120.

73. Pannier, M., Veit, S., Godt, A., Jeschke, G., and Spiess, H.W. (2000). Dead-time Free Measurement of Dipole-Dipole Interactions between Electron Spins. J. Magn. Reson. (San Diego, Calif. : 1997) *142*, 331–340. https://doi.org/10.1006/jmre.1999.1944.

74. Kerry, P.S., Turkington, H.L., Ackermann, K., Jameison, S.A., and Bode, B.E. (2014). Analysis of influenza A virus NS1 dimer interfaces in solution by pulse EPR distance measurements. J. Phys. Chem. B *118*, 10882–10888. https://doi.org/10.1021/jp508386r.

75. Jeschke, G., Sajid, M., Schulte, M., and Godt, A. (2009). Three-spin correlations in double electron-electron resonance. Phys. Chem. Chem. Phys. *11*, 6580–6591. https://doi.org/10.1039/b905724b.

76. Tait, C.E., and Stoll, S. (2016). Coherent pump pulses in Double Electron Electron Resonance spectroscopy. Phys. Chem. Chem. Phys. *18*, 18470–18485. https://doi.org/10.1039/c6cp03555h.

77. Jeschke, G., Chechik, V., Ionita, P., Godt, A., Zimmermann, H., Banham, J., Timmel, C.R., Hilger, D., and Jung, H. (2006). DeerAnalysis2006—a comprehensive software package for analyzing pulsed ELDOR data. Appl. Magn. Reson. *30*, 473–498. https://doi.org/10.1007/bf03166213.

78. Schiemann, O., Heubach, C.A., Abdullin, D., Ackermann, K., Azarkh, M., Bagryanskaya, E.G., Drescher, M., Endeward, B., Freed, J.H., Galazzo, L., et al. (2021). Benchmark Test and Guidelines for DEER/PELDOR

Experiments on Nitroxide-Labeled Biomolecules. J. Am. Chem. Soc. *143*, 17875–17890. https://doi.org/10.1021/jacs.1c07371.

79. Fábregas Ibáñez, L., Jeschke, G., and Stoll, S. (2020). DeerLab: a comprehensive software package for analyzing dipolar electron paramagnetic resonance spectroscopy data. Magn. Reson. *1*, 209–224. https://doi.org/10.5194/mr-1-209-2020.
80. Hagelueken, G., Abdullin, D., and Schiemann, O. (2015). mtsslSuite: Probing Biomolecular Conformation by Spin-Labeling Studies. Methods Enzymol. *563*, 595–622. https://doi.org/10.1016/bs.mie.2015.06.006.
81. Schanda, P., Kupce, E., and Brutscher, B. (2005). SOFAST-HMQC experiments for recording two-dimensional heteronuclear correlation spectra of proteins within a few seconds. J. Biomol. NMR *33*, 199–211. https://doi.org/10.1007/s10858-005-4425-x.
82. Delaglio, F., Grzesiek, S., Vuister, G.W., Zhu, G., Pfeifer, J., and Bax, A. (1995). NMRPipe: a multidimensional spectral processing system based on UNIX pipes. J. Biomol. NMR *6*, 277–293. https://doi.org/10.1007/BF00197809.

STAR★METHODS

KEY RESOURCES TABLE

REAGENT or RESOURCE	SOURCE	IDENTIFIER
Bacterial and virus strains		
MJF612 *E. coli* strain	Levina et al.[4] Edwards et al.[29]	N/A
Chemicals, peptides, and recombinant proteins		
N-Dodecyl-b-D-Maltopyranoside (DDM), anagrade	Anatrace or Glycon	Cat# D310 or D97002
1-Oxyl-2,2,5,5-tetramethyl-3-pyrroline-3-methyl)methanethiosulfonate (MTSSL)	Santa Cruz or Toronto Research Chemicals	Cat# 81213-52-7 or O875000
dioleoyl-sn-glycero-3-phosphocholine (DOPC)	Anatrace	Cat# 850375
β-cyclodextrin	Thermo Scientific	Cat# 406001000
Critical commercial assays		
Ni-NTA Agarose Resin	Invitrogen	Cat# R901-15
Superdex 200 Increase 10/300 GL column	Cytiva	Cat# 28-9909-44
Deposited data		
EPR data	This Paper	Database: https://doi.org/10.5518/1267
NMR data	This Paper	Database: https://doi.org/10.5518/1267
Atomic coordinates and structural factors: open MscS	Pliotas et al.[9]	PDB: 5AJI
Atomic coordinates and structural factors: subconducting MscS	Zhang et al.[14]	PDB: 6VYL
Atomic coordinates and structural factors: closed MscS	Zhang et al.[14]	PDB: 6VYK
Atomic coordinates and structural factors: desensitized MscS	Zhang et al.[14]	PDB: 6VYM
Oligonucleotides		
Primer: MscS D67C Forward TGTTTTCTTTCTGCATTAGTCCGTTACG	This Paper	N/A
Primer: MscS D67C Reverse AAGAAAACAAGCAACAGTGGCATCGATTTTACG	This Paper	N/A
Primer: MscS M47C Forward TGCATTTCCAACGCGGTGAATCGC	This Paper	N/A
Primer MscS M47C Reverse TTGGAAATGCACCGCGCGATAATCAAACCAAC	This Paper	N/A
Recombinant DNA		
Plasmid: pTRCMscSLE6xHis	Levina et al.[4]	N/A
Software and algorithms		
DeerAnalysis	Jeschke et al.[77]	https://epr.ethz.ch/software.html
ComparativeDEERAnalyzer (CDA) version 2.0	Schiemann et al.[78] Fabregas et al.[79]	https://epr.ethz.ch/software.html
mtsslSuite	Hagelueken et al.[80]	http://www.mtsslsuite.isb.ukbonn.de/
nmrPipe	Delaglio et al.[82]	https://www.ibbr.umd.edu/nmrpipe/index.html
Clampfit 10.7	Molecular Devices	https://support.moleculardevices.com/s/article/Axon-pCLAMP-10-Electrophysiology-Data-Acquisition-Analysis-Software-Download-Page
Origin 2018b	OriginLab Corporation	https://www.originlab.com/index.aspx?go=PRODUCTS/Origin
CHARMM-GUI	Jo et al.[65]	https://www.charmm-gui.org/
Code to analyze NMR data	This Paper	Database: https://doi.org/10.5518/1267

(*Continued on next page*)

Continued

REAGENT or RESOURCE	SOURCE	IDENTIFIER
Other		
Vivaspin-2 (100 kDa MWCO) Concentrator	Sartorius	Cat# VS0241
Bio-Beads SM-2 Adsorbents	Bio-Rad	Cat# 1523920

RESOURCE AVAILABILITY

Lead contact

Further information and requests for resources and reagents should be directed to and will be fulfilled by the lead contact, Christos Pliotas (christos.pliotas@manchester.ac.uk).

Material availability

All unique reagents generated in this study are available from the lead contact upon reasonable request.

Data and code availability

- Datasets are publicly accessible and are available through the following link: https://doi.org/10.5518/1267.
- Code used to analyze the NMR data is publicly accessible and available through the following link: https://doi.org/10.5518/1267.
- Any additional information required to reanalyze the data reported is available from the lead contact upon request.

EXPERIMENTAL MODEL AND STUDY PARTICIPANT DETAILS

Plasmid propagation was performed using DH5α competent E. coli cells plated on Luria Broth (LB) agar (37°C) or inoculated in LB liquid media (37°C, 200 RPM); both grown overnight in the presence of a selective antibiotic. Recombinant MscS and associated mutants were produced in E. coli MJF612,[4,29] cultured in LB Broth supplemented with selective antibiotic for 4 h (25°C, 200 RPM) following IPTG induction (final concentration 1 mM) at an OD600 ∼0.8. Full details are available in the STAR Methods text.

METHOD DETAILS

Expression, purification, and spin labeling of MscS

MscS constructs (WT or Cys variants) were transformed into the Escherichia coli strain MJF612[4,29] (ΔyggB, ΔmscL, ΔmscK, and ΔybdG). Cells were grown in 500 mL of LB medium at 37°C to an OD600 nm ≈ 0.8. The cultures were cooled to 25°C and induced with 1 mM IPTG for 4 h. The cell pellet was resuspended in PBS buffer (phosphate-buffered saline buffer, pH 7.5: containing 8 g of NaCl, 0.2 g of KCl, 1.15 g of $Na_2HPO_4 \cdot 7H_2O$, and 0.2 g of KH_2PO_4 per liter), supplemented with 0.2 mM freshly prepared phenylmethylsulfonylfluoride (PMSF). After cell disruption, the suspension was centrifuged at 4,000 × g for 30 min to remove cell debris. The supernatant was then centrifuged at 100,000 × g for 1 h. The membrane pellet was resuspended in solubilization buffer containing 1.5% DDM (n-dodecyl-beta-D-maltoside), 50 mM sodium phosphate pH 7.5, 300 mM NaCl, 10% glycerol, 50 mM imidazole, 0.2 mM PMSF (phenylmethylsulfonyl fluoride), and complete EDTA-free protease inhibitor (Merck) and incubated at 4°C. Non-solubilized membrane proteins were removed by centrifugation at 4,000 × g for 30 min, and the supernatant was passed through a 15-mL column containing 0.5 mL of nickel-nitrilotriacetic acid (Ni-NTA) agarose. The column was washed with 10 mL of wash buffer (0.05% DDM, 50 mM sodium phosphate pH 7.5, 300 mM NaCl, 10% glycerol, 50 mM imidazole) to remove non-specifically bound proteins. Spin labeling was performed and efficiency was assessed as previously described.[51,70–72] Briefly, TCEP (Tris-(2-carboxyethyl)-phosphine) dissolved in wash buffer was then added to briefly reduce MscS cysteines and subsequently MTSSL (1-Oxyl-2,2,5,5-tetramethyl-3-pyrroline-3-methyl)methanethiosulfonate) dissolved in wash buffer was added at a concentration 10× in excess of the expected protein concentration and left to react o/night at 4°C. The next morning freshly made MTSSL solution of the same concentration dissolved in wash buffer was added to the column and left to react for another 1 h. Finally, the protein was eluted with 10 mL of elution buffer (0.05% DDM, 50 mM sodium phosphate pH 7.5, 300 mM NaCl, 10% glycerol, 300 mM imidazole), and 1 mL fractions were collected. The eluted protein was concentrated to 0.8 ml and subjected to size exclusion chromatography (SEC) using a Superdex 200 Increase column (Cytiva) with the SEC buffer (50 mM sodium phosphate at pH 7.5, 300 mM NaCl and 0.05% w/v DDM). Following SEC, the MscS protein sample was ready for reconstitution into NDs.

MscS reconstitution into nanodics

MSP1D1E3 was the membrane scaffold belt protein used for reconstitution with 1,2-dioleoyl-sn-glycero-3-phosphocholine (DOPC) lipids. Prior to reconstitution, DOPC was solubilized in 50 mM sodium phosphate at pH 7.5, 300 mM NaCl, 1% w/v DDM using sonication. MscS, MSP1D1E3, and DOPC were then mixed at the molar ratio of 1:10:1000 and incubated on a roller for 30 mins. The

detergent was then extracted using Bio-Beads (Bio-Rad) and left overnight on a roller at room temperature (RT). The following day, a Hamilton syringe was used to remove the sample from the Bio-Beads.

Treatment of MscS-containing NDs with CD

To create a stock concentration of ~200 mM, CD was dissolved in 50 mM sodium phosphate solution pH 7.5, 300 mM sodium chloride. The MscS reconstituted NDs were treated with 10 mM CD for 4 h and 16 h, 30 mM and 60 mM CD for 16 h at RT. The final concentration of the DOPC in NDs was ~4.52 mM. After incubation, the empty lipid NDs and aggregated species were separated from the CD MscS-ND using SEC on a Superdex 200 Increase (Cytiva) column. For subsequent PELDOR analysis, the fractions of MscS reconstituted NDs were gathered and concentrated to ~40 μl.

PELDOR (or DEER) spectroscopy

For PELDOR measurements, MscS samples were diluted 1:1 with deuterated ethylene glycol, and 70 μL of the mixture was loaded in 3 mm (OD) quartz tubes and snap-frozen in liquid N_2. PELDOR experiments were performed at Q-band frequency (34 GHz) operating on a Bruker ELEXSYS E580 spectrometer with a 3 mm cylindrical resonator (ER 5106QT-2w). Pulses were amplified by a pulse traveling wave tube (TWT) amplifier (Applied Systems Engineering) with a nominal output of 150 W. The temperature was controlled via a cryogen-free variable temperature cryostat (Cryogenic Ltd) operating in the 3.5 to 300 K temperature range. PELDOR experiments were performed with the 4-pulse DEER[73] pulse sequence ($\pi/2(\upsilon_A) - \tau_1 - \pi(\upsilon_A) - (\tau_1 + t) - \pi(\upsilon_B) - (\tau_2 - t) - \pi(\upsilon_A) - \tau_2 -$ echo) at 50 K as described previously,[74] with a frequency offset (pump – detection frequency) of +80 MHz (~3 mT) and two step phase cycling of the first pulse. Shot repetition times (SRT) were set to 1.5 or 2 ms; t_1 was set to 380 ns, and t_2 was set to 2200 ns for the D67R1 mutant and to 2400 ns for the M47R1 mutant of MscS. Pulse lengths were 16 and 32 ns for $\pi/2$ and π detection. Measurements were performed with a reduced inversion efficiency[75] of 2/3 λ (probability of pumping spins) to minimize multispin effects.[61,62] For D67R1, an ELDOR π pump pulse of 20 ns was determined to achieve 2/3 l at 0 dB ELDOR attenuation; for M47R1 measurements were performed using rectangular pulses from an arbitrary waveform generator (AWG, Bruker) instead of the 2nd frequency ELDOR source, here a 12 ns pump pulse ELDOR pulse width was chosen to correspond to 2/3 λ and a 16-step phase cycle[76] was used. The pump pulse was placed on the resonance frequency of the resonator and applied to the maximum of the nitroxide field-swept spectrum. A 16-step nuclear modulation averaging (Δt = 8 ns) cycle was used for all experiments. Experiments ran typically 16 to 24 hrs.

As the challenging phase memory time and broad distance distribution make full resolution of the distance distribution very costly, we opted to record time domain data to excellent signal-to-noise ratio and correlate experimental trends in the primary data with predictions. For semi-quantitative analysis of primary PELDOR data, experimental traces for each mutant were rescaled using the modulation depth scaling tool (compare_modnorm) within DeerAnalysis,[77] with the control (no β-CD added) as the reference trace. Resulting scaled traces were processed using the ComparativeDEERAnalyzer (CDA) version 2.0[78,79] within DeerAnalysis2022 assuming a 7-spin system. The CDA reports containing further details on modulation depth, signal-to-noise ratio etc. can be accessed with the raw data. Distance distributions for the different MscS states (open: PDB 5AJI,[9] subconducting: PDB 6VYL, closed: PDB 6VYK,[14] desensitized: PDB 6VYM[14]) were modeled using mtsslSuite[80] and used to simulate time traces (not taking multi-spin effects into account) which were further scaled using the experimental modulation depth of the control sample for each mutant. These simulated scaled traces were compared with the experimental scaled primary PELDOR data for estimating the relative amount of open vs. closed; in addition, experimental and simulated difference traces were calculated to demonstrate a similar trend. Raw PELDOR traces are available at https://doi.org/10.5518/1267.

Sample preparation for NMR spectroscopy

Following the reconstitution of MscS D67C into MSP1D1E3 NDs, the sample was subjected to SEC with a Superdex 200 Increase column to separate MscS-ND from aggregation and empty NDs. MscS NDs were then concentrated to ~200 μl, using a 100 kDa cut-off, D_2O was added so that it was 5% of the final sample, and just before the NMR measurements, the sample was mixed with the 2:1 CD to lipid ratio. Immediately following the addition of CD, the sample was inserted into the NMR spectrometer and data acquisition was started. For empty (without MscS) NDs, following the reconstitution of DOPC into MSP1D1E3, samples were subjected to SEC using a Superdex 200 Increase column to separate the empty NDs from aggregated species. The sample was concentrated to ~200 μl and incubated with CD to lipid at 2:1, 6:1 and 12:1 ratios, equivalent to the PELDOR experiments. Immediately after the addition of CD, the sample was inserted into the NMR spectrometer and data acquisition was started as described below.

NMR spectroscopy

For real-time NMR, following the addition of CD series of SOFAST ^1H–^{13}C HMQC spectra[81] were recorded at 25°C, with acquisition times of 14 and 50 ms in t1 and t2 respectively and 16 or 32 scans per increment, resulting in an acquisition time of 15 or 30 min per spectrum. All data were collected on a Bruker Avance III spectrometer performing at a ^1H frequency of 950 MHz, equipped with a 3 mm TCI or 5 mm TXO probe. Data were processed and peak picked using nmrPipe.[82] Peak positions and intensities were fitted to a three-parameter exponential:

$$y = ae^{-\beta t} + c \quad \text{(Equation 1)}$$

where β is the exponential rate, a is the amplitude and c is the post-transition baseline, using custom scripts written in Python available at https://doi.org/10.5518/1267.

MscS reconstitution into proteoliposomes

Protocols followed were previously described here.[21] In brief, 200 μL of 10 mg/mL 20% Soy PC (Avanti) stock dissolved in chloroform was dried in a small glass vial under nitrogen flow. While drying the lipids, the vial was slowly rotated until a thin lipid layer film was formed. 500 μL of lipids buffer (containing 50 mM sodium phosphate buffer of pH 7.5 and 300 mM NaCl) were added into the vial, and the mixture was sonicated for 30 min until the solution was transparent. After the addition of DDM at a final concentration of 0.02%, purified protein samples and liposome solutions were mixed in a weight ratio (1:150) at RT for 1 h. Lipid buffer was left incubating with 300 mg of prewetted Bio-beads (Bio-Rad) at 4°C overnight. After the removal of Bio-beads, the mixture was centrifuged at 100,000 × g for 1 h. The resulting proteoliposome pellets were resuspended in 80 μL of lipid buffer, flash frozen in liquid-N_2 in 10-μL aliquots and stored at −80°C for future use.

GUVs formation and electrophysiology

Detailed protocols have been previously described here.[21] Briefly, pellet aliquots were thawed at RT, one day before the recordings, dehydrated overnight in a desiccator at 4°C and then rehydrated for 2 h at RT in rehydration buffer (50 mM sodium phosphate buffer pH 7.5, 300 mM NaCl, and 400 mM sucrose). 5 μL of the buffer containing GUVs were added to the center of a small petri dish (containing 2.5 ml of working solution: 5 mM HEPES pH 7.2, adjusted with KOH, 200 mM KCl, and 40 mM $MgCl_2$). Proteoliposomes were subsequently collapsed in the working solution and formed new giant blisters. Symmetrical ionic solutions were used in all recordings. Patch pipettes were pulled from thick-walled borosilicate glass capillaries (World Precision Instruments), which when filled with working solution had resistances of 3–6 MΩ. Single-channel currents were amplified using an Axopatch 200B amplifier (Molecular Devices). The currents were filtered at 1 kHz and sampled at 10 kHz with a Digidata 1440A using pClamp 10 software. Negative pressures were applied using a high-speed pressure clamp (HSPC-1, ALA Sciences).

Treatment of MscS-containing GUVs with CD

400 mM and 700 mM of β-cyclodextrin (CD) (Thermo Fisher Scientific) stocks were prepared by dissolving the powder into the working solution. Following multiple MscS channel openings elicited by negative pressure application, the protocol was immediately stopped and CD was added at respective ratios. Finally, a constant voltage was only applied (−30 or +30 mV) without any application of pressure.

QUANTIFICATION AND STATISTICAL ANALYSIS

For electrophysiology, amplitude histogram with Gaussian fit enabled the calculation of single-channel conductance in Clampfit 10.7. The p values are from comparison in an unpaired t-test and are indicated in figures; n represents individual patches; figures were made in Origin 2018b.